Tetrahedron 66 (2010) 9277–9285

Contents lists available at ScienceDirect

Tetrahedron

journal homepage: www.elsevier.com/locate/tet

Structural study of 8-azole derivatives of protoberberine alkaloids: experimental and quantum chemical approach

Lukáš Maier [a], Tomáš Šolomek [b], Matej Pipíška [a], Zdeněk Kříž [a], Marek Nečas [b], Radek Marek [a,b,*]

[a] National Center for Biomolecular Research, Masaryk University, Kamenice 5/A4, CZ-62500 Brno, Czech Republic
[b] Department of Chemistry, Masaryk University, Kamenice 5, CZ-62500 Brno, Czech Republic

ARTICLE INFO

Article history:
Received 20 April 2010
Received in revised form 26 August 2010
Accepted 13 September 2010
Available online 17 September 2010

Keywords:
Barrier to rotation
Berberine
Low-temperature NMR spectroscopy
Nucleus-independent chemical shift
Palmatine
Theoretical calculations

ABSTRACT

New derivatives of protoberberine alkaloids were prepared by nucleophilic addition of some azoles (differing in bulkiness) to the iminium functionality of the quaternary protoberberine alkaloids. Compounds were structurally characterized mainly by ^{1}H and ^{13}C NMR spectroscopy, and the structure of 8-carbazol-1-yl-7,8-dihydroberberine was determined using single-crystal X-ray diffraction. Additionally, conformational behaviors of five derivatives varying in bulkiness of the azole moiety have been investigated by low temperature NMR spectroscopy and quantum chemical calculations. Ring current effects of pyrrole and carbazole moieties on selected ^{1}H NMR resonances have been characterized, visualized, and discussed.

1. Introduction

Alkaloids represent a group of naturally occurring molecules being frequently studied for their interesting pharmacological effects. The group of quaternary protoberberine alkaloids (QPAs) belongs to the large family of isoquinolines. Compounds of the QPA group are, together with some other isoquinoline alkaloids, widely distributed in plant families Papaveraceae, Berberidaceae, Rutaceae, Ranunculaceae, etc.[1] The basic skeleton of QPA is 5,6-dihydrodibenzo[*a*,*g*]quinolizinium, which is usually stabilized by the anion of an organic acid or chloride. Substituents of the basic scaffold are limited mainly to hydroxy, methoxy, and methyl groups at several positions. The 2,3,9,10-tetrasubstituted QPAs represent the most abundant subgroup of QPAs. Berberine (1), palmatine (2), and coptisine (3) are the main representatives of this subgroup (Fig. 1). Various biological activities of natural QPAs and some synthetic derivatives of QPAs have been described in several papers.[2] It has been found that these compounds have substantial antibacterial, antifungal, antiviral, and antimalarial properties.[2]

They may inhibit certain metabolic pathways and interact with oligonucleotides and DNA.[3] However, pharmacological applications of these alkaloids are still restricted due to their high cytotoxicity.

Quaternary protoberberine alkaloids can react as electrophiles due to the presence of the iminium moiety.

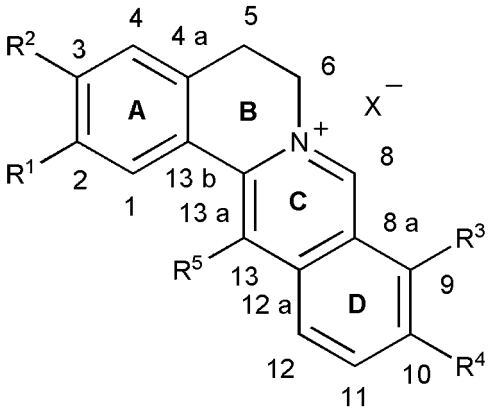

(1) : $R^1 + R^2 = OCH_2O$, $R^3 = R^4 = OCH_3$, $R^5 = H$
(2) : $R^1 = R^2 = R^3 = R^4 = OCH_3$, $R^5 = H$
(3) : $R^1 + R^2 = R^3 + R^4 = OCH_2O$, $R^5 = H$
(4) : $R^1 + R^2 = OCH_2O$, $R^3 = R^4 = OCH_3$, $R^5 = Bn$

Fig. 1. Structures of QPAs.

* Corresponding author. Fax: +420 549492556; e-mail address: rmarek@chemi.muni.cz (R. Marek).

0040-4020/$ – see front matter © 2010 Elsevier Ltd. All rights reserved.
doi:10.1016/j.tet.2010.09.030

Their reactions with Grignard reagents, cyanide, trichloromethyl anion, and oxygen nucleophiles,[4] yield 8-substituted dihydroprotoberberines. The stability of 7,8-dihydroprotoberberberine is highly dependent on the nature of the nucleophile. The stabilities of adducts formed by the addition of *C*-nucleophiles are significantly higher as compared to those containing O, N, or S linking atoms. The latter represent good leaving groups so the adducts can undergo additional chemical transformations towards the more thermodynamically stable molecules. Chemical transformations of 8-hydroxy derivatives of berberine and coptisine observed in solutions are good examples of this behavior.[4]

Very recently, we reported the successful preparation of covalent adducts of berberine, palmatine, and coptisine with sodium salts of some simple azoles and methanethiolate.[5] Extending our research effort in this field we communicate here an investigation into the addition of some bulky azoles, such as indole or carbazole, and the study of barriers to rotation around the newly created C–N bond. The conformational behavior is investigated also for the recently published 8-pyrrol-1-yl-7,8-dihydroberberine.[5]

Dynamic NMR spectroscopy has proven to be a powerful tool to study various dynamic processes in molecules ranging from small organics and organometallics to biological systems. Reversible intramolecular dynamic processes, such as rotation around a single bond, can be investigated experimentally by NMR techniques in solution and solid state.[6] The temperature dependent NMR experiments and correlation spectroscopy (e.g., EXSY) can be complemented by computational methods and molecular modeling.[7]

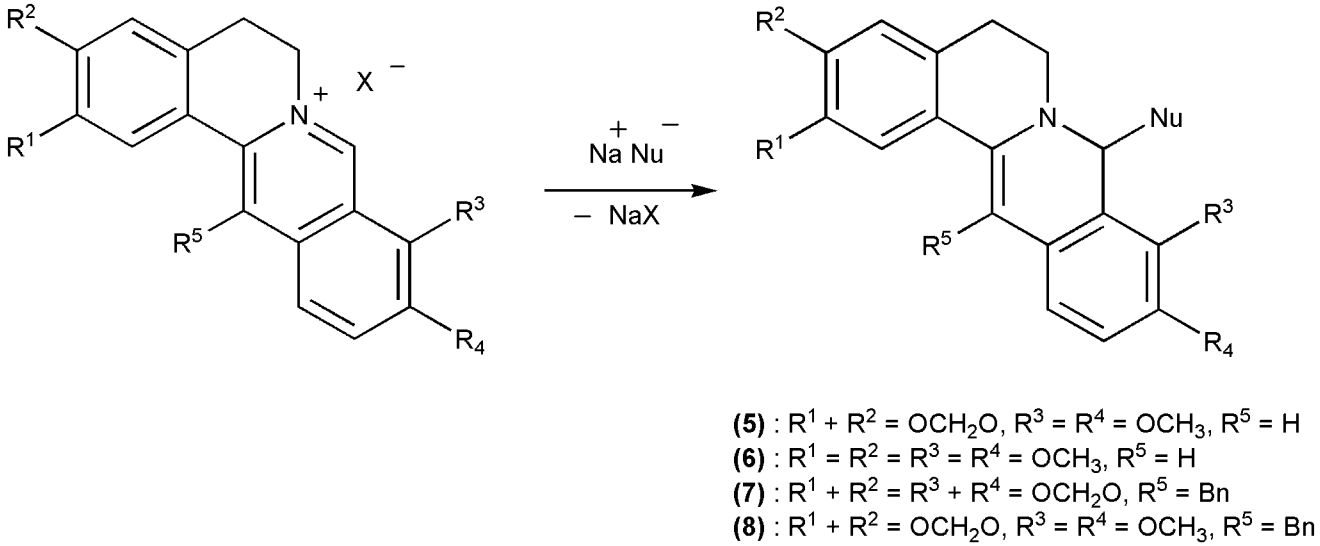

(5) : $R^1 + R^2 = OCH_2O$, $R^3 = R^4 = OCH_3$, $R^5 = H$
(6) : $R^1 = R^2 = R^3 = R^4 = OCH_3$, $R^5 = H$
(7) : $R^1 + R^2 = R^3 + R^4 = OCH_2O$, $R^5 = Bn$
(8) : $R^1 + R^2 = OCH_2O$, $R^3 = R^4 = OCH_3$, $R^5 = Bn$

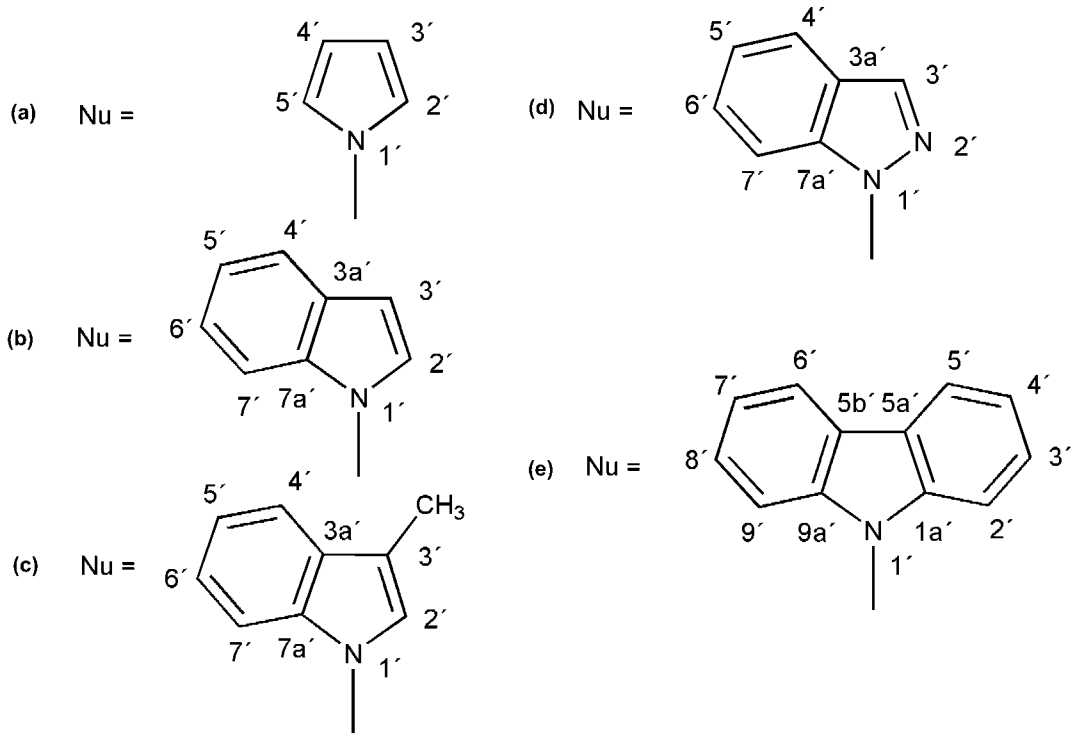

Fig. 2. The nucleophilic addition of azoles to the quaternary protoberberine skeleton.

An approach combining NMR spectroscopy and theoretical calculations is employed in this contribution.

2. Results and discussion

Preparation of 8-substituted derivatives of naturally occurring alkaloids berberine, coptisine, and palmatine is schematically depicted in Fig. 2. The sodium salt of the corresponding azole was prepared by reacting NaH with the azole in THF under an argon atmosphere. In the following step, the nitrogen atom of the salt attacked the electron deficient carbon of the iminium functionality resulting in C-8 substituted derivatives of 7,8-dihydroprotoberberine.

In order to investigate the influence of the substituents on this reaction, 13-benzylberberine bromide (compound **4**) was prepared according to the published procedure via well-known 8-acetonylberberine as a key intermediate[2] and was subjected to nucleophilic addition with some azoles.

MS analysis of the products was complicated by an extraordinary lability of the newly created C–N bond as reported very recently.[5] The reaction products were therefore characterized mainly by using NMR spectroscopy. All resonances in the ^{1}H and ^{13}C NMR spectra were completely assigned using COSY, NOESY, $^{1}H-^{13}C$ HMQC, $^{1}H-^{13}C$ HMBC, and $^{1}H-^{13}C$ GSQMBC experiments. Assignments of ^{1}H and ^{13}C resonances for compounds **4**–**8** are summarized in Tables 1 and 2, respectively.

Nucleophilic addition and the formation of 7,8-dihydroprotoberberine induce a substantial shift change for atoms H-8, H-13, C-8, and C-13 due to the loss of aromaticity of the C ring (Fig. 1). Similar to the trends observed for simple azoles,[5] the resonance of H-8 is shifted from 9.91 ppm for **1** to 7.2–7.8 for compounds **5**. ^{13}C NMR resonances are affected in a similar way, for example, the chemical shift of 145.37 ppm was observed for C-8 in berberine chloride, whereas C-8 in adducts resonate in the range 66–72 ppm. However, these values should be compared with caution because different solvents were used to measure QPAs and 7,8-dihydroprotoberberines. Observation of two chemically nonequivalent protons at positions C-5 and C-6 for compounds **5**–**8** correlates with the induction of the stereogenic center at position C-8.

The covalent attachment of azole to the protoberberine skeleton was supported by observing NOE interactions between protons of the protoberberine moiety and protons of the azole part. This was further confirmed for several compounds by detecting the long-range $^{1}H-^{13}C$ interactions between H-8 and some carbons of the azole part.

Resonances of C-2, C-3, C-9, and C-10 were assigned by interpreting the long-range $^{1}H-^{13}C$ coupling constants. For example, experimentally observed $^{2}J_{H4,C3}$=3.7 Hz for **7e** nicely corresponds to the DFT calculated value of 3.5 Hz. In contrast, $^{3}J_{H4,C2}$ is approximately twice as large compared to the $^{2}J_{H4,C3}$. The experimental value of $^{3}J_{H4,C2}$=7.2 Hz is again in agreement with theoretical prediction (7.3 Hz). A similar strategy based on the differences between $^{2}J_{H,C}$ and $^{3}J_{H,C}$ was applied for assigning C-9 and C-10 resonances.

It is interesting to note the exceptionally large substituent-induced shifts observed for H-8 and 9-OCH_3 resonances in adducts **5e** and **6e** and for H-8 in **7e**. More comprehensive discussion on this topic is provided in following sections.

Differences in selected ^{1}H NMR chemical shifts for compounds **5**–**7** are summarized in Table S1. A formal replacement of the pyrrole moiety by indole in compound **5** induces deshielding of H-8 by 0.61 ppm, whereas protons of the 9-OCH_3 group are shielded by 0.25 ppm. Data comparing pyrrole and carbazole fragments in compounds **5**–**7** indicate an even more pronounced influence of the aromatic rings. The deshielding of H-8 by 1.12 ppm could be rationalized by the position of H-8 in the plane of the carbazole moiety. In contrast, position of 9-OCH_3 group above the plane of aromatic π-system of carbazole moiety gives rise to shielding of approximately 0.6 ppm. The topological positions of H-8 and 9-OCH_3 estimated from NMR data have been supported by the solid-state molecular structure of compound **5e** determined by X-ray diffraction (Fig. 3) and quantum chemical calculations discussed below. Several structural features of 8-carbazol-1-yl-7,8-dihydroberberine (**5e**) deserve more detailed discussion.

Interatomic distance C8–N1′ (1.476 Å) is comparable with those obtained for several berberine adducts with azole rings.[5] The methoxy group at C-10 lies almost in the plane of aromatic ring D as previously found in the crystals of the quaternary protoberberines and QPA adducts with oxygen and nitrogen nucleophiles.[1,4,5]

The C9–OMe group is nearly perpendicular to the plane of ring D, interestingly in the position close to the carbazole part of molecule. The same orientation has been reported for the crystal structure of **5a** and 8-pyrazol-1-yl-7,8-dihydroberberine.[5] In contrast, the 9-OMe group is orientated reversely in the crystal structure of 8-trichlormethyl-7,8-dihydroberberine and 8-methoxy-7,8-dihydroberberine.[4c]

Very broad resonances in the aromatic region were found in ^{1}H NMR spectrum of 8-carbazol-1-yl-7,8-dihydroberberine (**5e**)

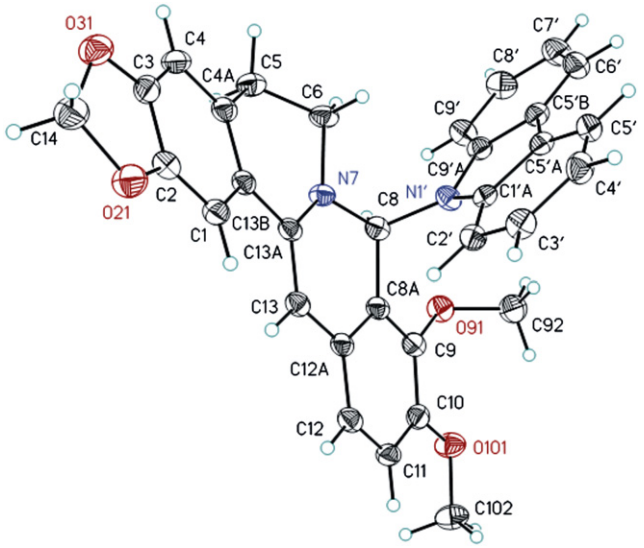

Fig. 3. The molecular structure of 8-(carbazol-1-yl)-7,8-dihydroberberine (**5e**) obtained from single-crystal X-ray diffraction.

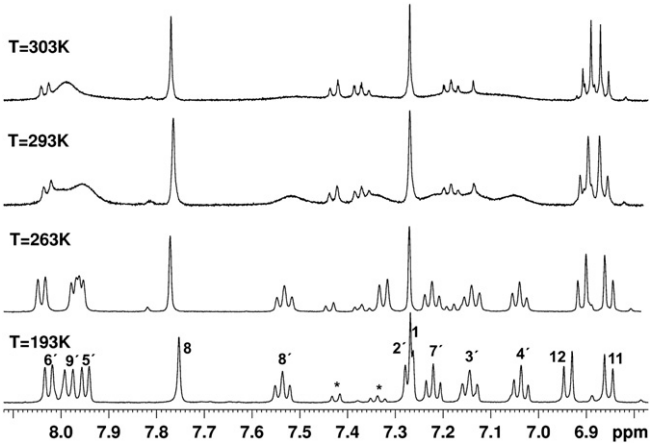

Fig. 4. A portion of the ^{1}H NMR spectrum for compound **5e** measured in CD_2Cl_2 at several temperatures (some signals of protons corresponding to the free 1*H*-carbazole, which was created after dissolving **5e** in CD_2Cl_2, are marked by an asterisk).

Table 1
^{1}H NMR chemical shifts (δ in ppm) for 13-benzylberberine bromide (**4** in DMSO-d_6) and 8-substituted 7,8-dihydroprotoberberines **5**–**8** (in CD_2Cl_2)

Atom	**5b**	**5c**	**5d**	**5e**	**6e**	**7e**	**4**	**8a**
	303 K	303 K	303 K	223 K[a]	223 K[a]	233 K[a]	303 K	303 K
H-1	7.23s	7.23s	7.22s	7.28s	7.26s	7.28s	6.98s	6.85s
H-4	6.51s	6.51s	6.51s	6.47s	6.48s	6.46s	7.17s	6.64s
H-5	2.55m	2.56m	2.53m	2.44m	2.44m	2.39m	3.17t	2.62m
	2.84m	2.84m	2.83m	2.82m	2.84m	2.79m	—	2.86m
H-6	2.84m	2.84m	2.83m	2.53m	2.58m	2.44m	4.89t	3.24m
	3.43m	3.41m	3.48m	3.23m	3.27m	3.13m	—	3.51m
H-8	7.29s	7.22s	7.53s	7.77s	7.80s	7.67s	10.04s	6.80s
H-11	6.95d	6.94d	6.95d	6.87d	6.87d	6.76d	8.10d	6.88d
H-12	6.99d	6.98d	6.98d	6.94d	6.94d	6.88d	7.79d	6.95d
H-13	6.19s	6.16s	6.20s	6.17s	6.24s	6.18s	—	—
2,3-OCH_2O/2-OCH_3	5.92d	5.92d	5.91d	5.93d	3.91s	5.93d	6.08s	5.86d
3-OCH_3	—	—	—	—	3.72s	—	—	—
9,10-OCH_2O/9-OCH_3	3.23s	3.22s	3.19s	2.67s	2.66s	5.72d	4.13s	3.46s
10-OCH_3	3.80s	3.80s	3.79s	3.69s	3.69s	—	4.03s	3.80s
H-2′	7.00d	6.73d	—	7.31d	7.34d	7.31d	—	6.67m
H-3′	6.33d	—	7.90s	7.16t	7.17t	7.18t	—	6.01m
H-3′-CH_3	—	2.14s	—	—	—	—	—	—
H-4′	7.52d	7.44d	7.48d	7.05t	7.06t	7. 09t	—	6.01m
H-5′	7.05t	7.04t	7.25t	7.96d	7.97d	7.99d	—	6.67m
H-6′	7.23t	7.22t	7.05t	8.04d	8.05d	8.05d	—	–
H-7′	7.76d	7.71d	7.63d	7.24t	7.24t	7.24t	—	—
H-8′	—	—	—	7.55t	7.55t	7.51t	—	—
H-9′	—	—	—	7.99d	8.00d	7.90d	—	—

[a] Signals are resolved and no spectral overlap was observed at this temperature.

Table 2
^{13}C NMR chemical shifts (δ in ppm) for 13-benzylberberine bromide (**4** in DMSO-d_6) and 8-substituted 7,8-dihydroprotoberberines **5**–**8** (in CD_2Cl_2)

Atom	**5b**	**5c**	**5d**	**5e**	**6e**	**7e**	**4**	**8a**
	303 K	303 K	303 K	263 K[a]	253 K[a]	253 K[a,b]	303 K	303 K
C-1	104.38	104.88	104.42	104.50	107.01	104.49	108.09	108.81
C-2	146.97	147.43	146.92	146.70	147.78	146.71	146.36	146.13
C-3	147.72	148.17	147.66	147.54	149.20	147.57	149.19	147.78
C-4	107.77	108.26	107.72	107.68	110.27	107.68	108.44	108.24
C-4a	127.70	128.18	124.46	129.11	127.50	129.04	129.98	128.13
C-5	29.80	30.33	29.79	29.41	29.03	29.29	27.24	31.85
C-6	46.51	46.98	46.10	44.89	45.10	44.52	56.97	49.22
C-8	66.50	66.50	71.54	66.72	66.96	66.17	145.42	69.69
C-8a	120.74	121.42	119.15	118.52	118.63	107.31	121.22	122.70
C-9	145.50	145.94	145.88	145.99	146.13	144.90	144.24	145.10
C-10	150.16	150.61	150.01	149.74	149.82	144.60	150.18	150.91
C-11	114.10	114.43	114.27	113.37	113.47	109.25	126.17	113.73
C-12	120.69	120.00	119.35	119.00	118.95	116.33	121.61	119.01
C-12a	128.06	128.67	129.19	128.29	128.59	128.89	132.75	133.37
C-13	94.71	95.09	94.47	92.19	91.71	92.37	134.02	104.64
C-13a	137.45	137.94	137.66	137.75	137.91	137.79	137.13	136.74
C-13b	125.05	125.60	125.01	124.48	122.74	124.34	119.97	126.03
2,3-OCH_2O/2-OCH_3	101.39	101.89	101.35	101.43	56.05	101.49	102.00	101.83
3-OCH_3	—	—	—	—	55.92	—	—	—
9,10-OCH_2O/9OCH_3	60.01	60.54	59.90	59.06	59.20	101.73	62.02	60.53
10-OCH_3	56.05	56.55	55.99	55.62	55.76	—	56.91	56.36
C-1a′	—	—	—	140.70	140.87	140.66	—	—
C-2′	126.79	124.46	—	112.82	110.90	112.54	—	—
C-3′	102.56	112.28	133.18	125.61	125.83	125.98	—	—
C-3′–CH_3	—	9.80	—	—	—	—	—	—
C-3a′	129.22	129.72	128.45	—	—	—	—	—
C-4′	119.59	119.25	110.77	119.22	119.39	119.97	—	—
C-5′	119.42	119.25	126.28	119.86	120.10	120.21	—	—
C-5a′	—	—	—	122.58	122.89	122.51	—	—
C-5b′	—	—	—	123.39	123.52	123.48	—	—
C-6′	121.82	122.27	120.54	120.16	120.38	120.34	—	—
C-7′	110.04	110.17	120.75	119.22	119.39	119.45	—	—
C-7a′	135.87	136.71	138.54	—	—	—	—	—
C-8′	—	—	—	125.80	126.02	125.98	—	—
C-9′	—	—	—	109.45	109.66	108.95	—	—
C-9a′	—	—	—	138.02	138.16	137.73	—	—

[a] Signals are resolved and no spectral overlap was observed at this temperature.
[b] Assignments of signals C-2, C-3, C-9, and C-10 were accomplished by interpreting the ^{1}H–^{13}C coupling constants.

measured at 303 K (see Fig. 4). Resonance broadening indicated a dynamic process occurring in the solution. Observation of this dynamic behavior initiated our interest in the conformational study of adducts in solution. The resonance broadening could be rationalized by slow hindered rotation of the carbazole moiety around the newly created C–N bond. Experimental NMR study and theoretical calculations were performed in order to confirm an assumed phenomenon of hindered rotation and to estimate the barriers to rotation. A portion of the ^{1}H NMR spectrum for **5e** measured at several low temperatures is shown in Fig. 4.

Temperature of coalescence for several of the ^{1}H NMR signals was estimated from these measurements. From chemical shifts for individual atoms observed at low temperatures, exchange rates and Gibbs activation energies ($\Delta G^{\ddagger}_{obs}$) of barriers to rotation were calculated by transition state theory.[8] The experimental values for **5e**, **6e**, and **7e** together with the calculated energies obtained by density functional theory (DFT) calculations are summarized in Table 3.

NOESY experiments were used as a supporting tool for the dynamic study and for the resonance assignment. Exchange signals between pairs of protons observed in the spectrum of **5e** at 263 K (Fig. 5a) facilitated resonance assignment. It allowed unequivocal assignments of protons of the carbazole moiety. Schematic representation of observed interactions can be found in Supplementary data (Fig. S1). In contrast, solely NOE interactions were observed in the NOESY experiment recorded at 193 K without any signs of exchange (Fig. 5b). This result clearly indicates that the rotation of carbazole moiety around the berberine part of molecule is slow enough at 193 K to obtain discrete resonances for all protons of the carbazole part of the molecule. Moreover, observed H-8/H-9′ NOE interaction allowed 3-D assignments of resonances for the carbazole frame. Analogous dynamic behavior was observed for palmatine and coptisine derivatives **6e** and **7e**.

Despite relatively sharp resonances observed in the ^{1}H NMR spectrum of 8-indol-1-yl-7,8-dihydroberberine (**5b**) at 303 K, we performed temperature dependent ^{1}H NMR experiments (Fig. S2). Since C–N rotation for compound **5b** possesses lower symmetry than those for **5a** and **5e**, NMR signals belonging to two rotamers differing in energy might be detected at low temperatures. The NMR signals at 303 K represent time-averaged and population-weighted contributions of individual conformers. Signals are well resolved still at 253 K, but upon cooling the sample, we observed signal broadening for H-7′ and H-2′ at 223 K and 203 K, respectively. H-7′ and H-2′ are clearly the protons most influenced by the rotation of the indole moiety around the C–N bond. Finally, we observed relatively sharp signals again at 183 K. Unfortunately, we were not able to identify the resonances of the minor component probably due to its low population (for calculated energies, see theoretical study) in solution and the overlapping signals in the crowded aromatic spectral region. Therefore, $\Delta G^{\ddagger}_{obs}$ for **5b** is missing from Table 3.

Table 3
Rate constants (k_{obs}) determined experimentally by temperature dependent ^{1}H NMR spectroscopy and corresponding barriers to rotation obtained experimentally ($\Delta G^{\ddagger}_{obs}$) and calculated by DFT ($\Delta G^{\ddagger}_{calcd}$, 298 K)

Compound	k_{obs}/s^{-1}	$\Delta G^{\ddagger}_{obs}$ (kcal/mol)	$\Delta G^{\ddagger}_{calcd}$ (kcal/mol)
5a	—[a]	—[a]	4.66
5b	—[a]	—[a]	10.66
5e	86.47^{293K}	14.56^{293K}	14.96
6e	85.11^{298K}	14.83^{298K}	—[b]
7e	30.67^{288K}	14.43^{288K}	13.78

[a] Not determined experimentally.
[b] Not calculated theoretically.

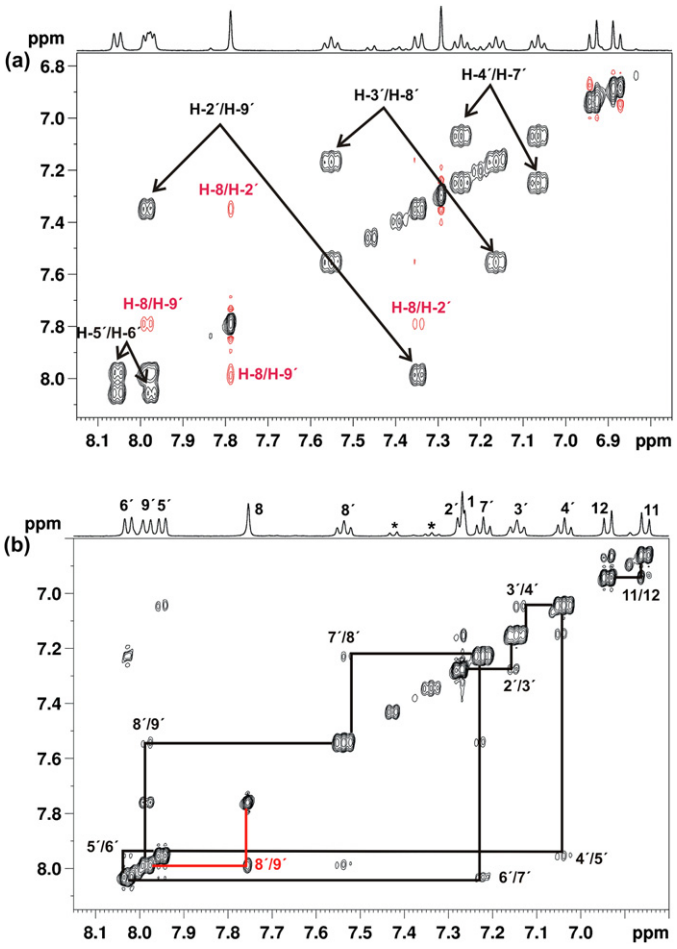

Fig. 5. A portion of the NOESY spectrum (mixing time 700 ms) for compound **5e**. (a) T=263 K with assignment of exchange signals for carbazole moiety (b) T=193 K with assignment of NOE signals.

The methyl group in the indole moiety has vanishingly small effect on the dynamic behavior as indicated by comparative low-temperature NMR study of **5c**.

2.1. Theoretical study of barriers to rotation

To get a deeper insight into the conformational behavior of selected compounds, we employed quantum chemical calculations to obtain the rotational barriers in compounds 8-pyrrol-1-yl-7,8-dihydroberberine (**5a**),[5] 8-indol-1-yl-7,8-dihydroberberine (**5b**), 8-carbazol-1-yl-7,8-dihydroberberine (**5e**), and 8-carbazol-1-yl-7,8-dihydrocoptisine (**7e**). The energy profile of the conformational motion was simulated by performing a relaxed potential energy surface scan by increasing the dihedral angle θ=N7–C8–N1′–C2′ with an increment of 10° over 180° in the case of **5a**, **5e**, **7e**, and 360° for **5b**.

The energy minimum for 8-pyrrol-1-yl-7,8-dihydroberberine (**5a**) has been found for the angle θ=115.0°. The structure of the most stable conformer is in very good agreement with that obtained from the X-ray diffraction data (θ=110.4°).[5] We located a transition state of the pyrrole moiety rotation with a rotational barrier $\Delta G^{\ddagger}_{calcd}$ (at 298 K) of 4.66 kcal mol^{-1} (Table 3).

The potential energy profile for 8-indol-1-yl-7,8-dihydroberberine (**5b**) is more complicated and as expected, four energy minima were found. The most stable conformer possesses the angle θ=60.1°. The benzene ring of the indole moiety is directed

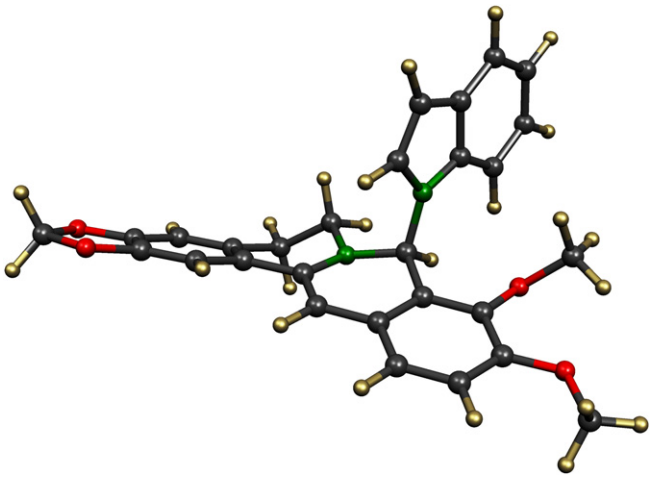

Fig. 6. The most stable conformer of 8-indol-1-yl-7,8-dihydroberberine (**5b**).

outside the molecule while the 9-OMe group is orientated towards the indole part as mentioned previously (Fig. 6).

Another significant conformation (1.16 kcal mol^{-1} higher in energy) shares almost the same orientation of the indole moiety (θ=54.1°) but interestingly, the 9-OMe group is orientated the other way around. The conformer with the reverse orientation of the indole moiety (θ=−119.6°) and the 9-OMe group pointing towards the indole and the last minor conformer (θ=−125.5°, 9-OMe group is reversed) are higher in energy by 2.29 and 3.42 kcal mol^{-1}, respectively. The structures together with the corresponding energies are given in Fig. S3. The overall barrier to rotation of 10.66 kcal mol^{-1} has been found for indol-1-yl-7,8-dihydroberberine (**5b**) (Table 3).

The most stable conformer of 8-carbazol-1-yl-7,8-dihydroberberine (**5e**) is defined by the angle θ=57.4°. Exactly the same value has been measured in the X-ray diffraction experiment of **5**e. The C9—OMe is nearly perpendicular to the ring D and is orientated towards the carbazole part the same way as observed in the crystal. The overall barrier to rotation of 14.96 kcal mol^{-1} has been calculated for **5e** (Table 3). This is in excellent agreement with the value of 14.56 kcal mol^{-1} obtained from the experiment.

The energy minimum for 8-carbazol-1-yl-7,8-dihydrocoptisine (**7e**) corresponds to the angle θ=51.9° and an overall barrier to rotation of 13.78 kcal mol^{-1} has been calculated. This is also in very good agreement with the experimentally observed value of 14.43 kcal mol^{-1}.

2.2. Interpretation of chemical shifts

Finally, we calculated ^{1}H NMR chemical shifts with respect to tetramethylsilane for **5a**, **5b**, and **5e** in order to support our structure elucidation and to obtain additional information about

Table 4
Experimental and calculated ^{1}H NMR chemical shifts for compounds **5**

	H-8		9-OMe		10-OMe	
	EXP[a]	CALC[b]	EXP[a]	CALC[b]	EXP[a]	CALC[b]
a^{303K}	6.68[c]	6.55	3.48[c]	3.31	3.83[c]	3.78
b^{303K}	7.29	7.20	3.23	3.05	3.80	3.77
e^{300K}	7.80	7.76	2.85	2.82	3.73	3.71
Δ (**b**−**a**)	0.61	0.65	−0.25	−0.26	−0.03	−0.01
Δ (**e**−**b**)	0.51	0.56	−0.38	−0.23	−0.07	−0.06
Δ (**e**−**a**)	1.12	1.21	−0.63	−0.49	−0.10	−0.07

[a] Experimentally observed data.
[b] B3LYP/6-31G(d,p), PCM solvent model//B3LYP/6-31G(d) geometry; referenced to TMS.
[c] Previously reported experimental data.[5]

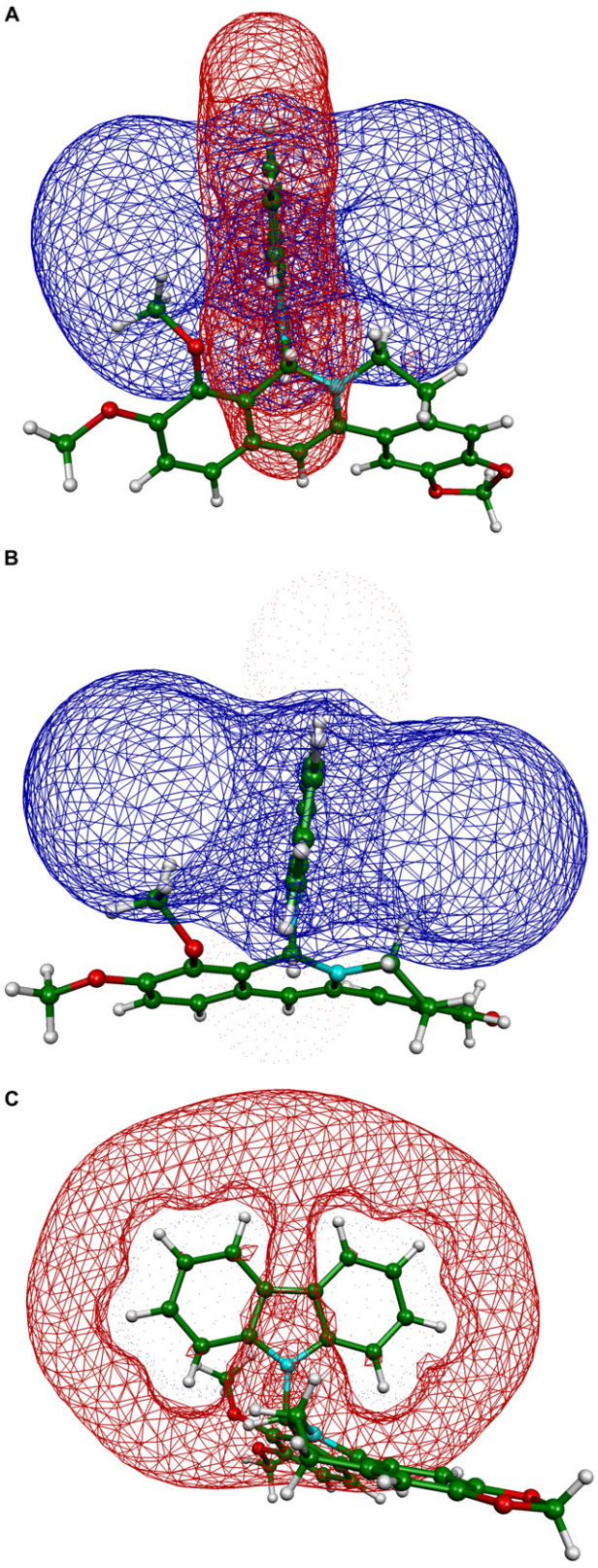

Fig. 7. Visualization of the differential NICS matrix between carbazole and pyrrole in coordination system of **5e**. Blue area represents a shielding region whereas red surface maps a deshielding sphere (cutoff±0.28 ppm). (A) Total view; (B) shielding region incorporating 9-OMe group; (C) deshielding region embedding H-8 atom.

electronic distribution in these molecules. Selected ^{1}H NMR chemical shifts calculated using B3LYP are summarized in Table 4 and compared with those observed experimentally.

Note that only the most stable conformer for each compound has been considered and no averaging has been attempted for simplicity. This approach has been shown to give reasonable results in some cases.[9] Although a small basis set (3-21G(d)) was initially used for the geometry optimization, the data computed for **5a**, **5b**, and **5e** correspond nicely to the experimentally observed values of chemical shifts with only slight deviations in some cases (see Table S2). Values for H-8 and C10–OMe are in excellent agreement with experiment while those computed for the C9–OMe group differ slightly.

To improve the agreement between the calculated chemical shifts and the experimental data for the 9-OMe group in **5a**, **5b**, and **5e**, a more accurate geometry optimized with 6-31G(d) basis set had to be used. By employing a new geometry, the agreement between theoretical and experimental data for 9-OCH_3 was significantly improved (compare Table 4 and Table S2).

It is evident from Table 4 that substantial differences in the chemical shifts for H-8 and 9-OMe are induced by the 'ring current' effects of pyrrole, indole, and carbazole. This 'through-space' effect was investigated in detail theoretically by calculating the nucleus-independent chemical shift (NICS)[10] and also by visualizing the *iso*-NICS surfaces.[10b] To investigate the differences between pyrrole (**a**) and carbazole (**e**) derivatives as examples, we calculated differential matrix of the *iso*-NICS values between free carbazole and pyrrole (see section Experimental). The resulting differential *iso*-NICS surface in coordination system of **5e** is shown in Fig. 7.

Protons of the 9-OMe group are clearly embedded in the shielding region (blue surface in Fig. 7), which results in the significant shielding of these protons in **5e** as compared to those in **5a** (experimental $\Delta\delta$=−0.63 ppm, see Table 4). In contrast, H-8 is located in the deshielding region (see Fig. 7c) with experimentally measured $\Delta\delta$=+1.12 ppm.

3. Conclusion

In summary, new derivatives of protoberberines were synthesized by the nucleophilic addition of sodium salts of azoles to quaternary protoberberine alkaloids. Detailed structural study with estimation of barriers to rotation around the C–N bond has been accomplished. The experimentally observed data obtained by low-temperature NMR spectroscopy and single-crystal X-ray diffraction analysis are nicely supported by the quantum chemical calculations. Although partly hindered, the reactive C=N$^+$ bond is accessible even for relatively bulky groups like carbazole and probably also for the purine bases of nucleic acids, which will be the subject of our future study.

4. Experimental

4.1. Reagents and techniques

Berberine chloride hydrate (Fluka), palmatine chloride hydrate (Sigma–Aldrich), and coptisine isolated from natural sources as chloride[5] were dried in oven (90 °C, 4 h) before using. Nitrogen heterocycles and other reagents were purchased from Sigma–Aldrich and were used without further purification. THF was distilled from Na with benzophenone prior to use.

EI mass spectra were measured using TRIO 1000 quadrupole mass spectrometer, Finnigan MAT (Fisons Instrument, San Jose, CAN, USA). MS analyses were performed by electron ionization technique (EI) with a direct insertion probe (DIP) used in EI$^+$ ionization mode, applying electron energy 30 eV. ESI-MS were collected using an Agilent HP 1100 LC/MSD Trap VL Series in MeOH, using direct infusion with a linear pump (kd Electronics) at a flow rate of 300 μL min^{-1}. The spectra were collected in positive mode, with the nebulizing and drying gas N_2 (300 °C) at a flow rate of 10 L min^{-1}, a nebulizer pressure of 80 psi, and a capillary voltage 3.5 kV. The full mass scan covered the range from *m*/*z* 200 to 1500.

IR spectra were measured by DRIFTIR method on Bruker VERTEX80v instrument. HR mass spectra were measured using APEX-Ultra FTMS instrument equipped with a 9.4 T superconducting magnet and a Dual II ESI/MALDI ion source (Bruker Daltonics, Billerica MA) using nano-assisted laser desorption/ionization (NALDI).

4.2. NMR spectroscopy

NMR spectra were recorded on a Bruker Avance 300 spectrometer operating at frequencies of 300.13 MHz (^{1}H) and 75.48 MHz (^{13}C) and a Bruker Avance 500 spectrometer operating at frequencies of 500.13 MHz (^{1}H) and 125.77 (^{13}C). The ^{1}H and ^{13}C NMR chemical shifts were referenced to the signal of CD_2Cl_2 [5.31 ppm (^{1}H) and 53.80 ppm (^{13}C)] and DMSO-d_6 [2.50 ppm (^{1}H) and 39.50 ppm (^{13}C)]. The temperature was calibrated using methanol sample. Mixing time t_m in NOESY experiment[11] was 700 ms, 500 ms, or 300 ms. ^{1}H–^{13}C HMQC experiments[12] were adjusted to $^1J_{H,C}$=150 Hz. ^{1}H–^{13}C HMBC[13] and ^{1}H–^{13}C GSQMBC[14] experiments were adjusted to $^nJ_{H,C}$=7.5 Hz or 4.2 Hz.

4.3. X-ray diffraction

Diffraction data were collected on a KUMA KM4CCD four-circle diffractometer (Oxford Diffraction, Abingdon, UK) equipped with a Cryostream low-temperature device (Oxford Cryosystems, Oxford, UK). The crystallographic package ShelXTL[15] was used to solve and refine the structure[16] of compound **5e**.

4.4. Synthesis

*4.4.1. 13-Benzylberberine bromide (**4**)*[2]. A round-bottomed flask (50 mL) was charged with 8-acetonylberberine (0.7970 g, 2 mmol) dissolved in acetonitrile (10 mL). Benzylbromide (1.5 equiv, 0.513 g) was added and the reaction mixture was refluxed for 6 h. The reaction mixture was cooled down to room temperature and solvent was evaporated under vacuum. The dark yellow residue was dissolved in $CHCl_3$ and pre-adsorbed on alumina. Pure product was obtained by column-chromatography using $CHCl_3$ as eluent system.

Yield: 50% of yellow solid; mp: ~200 °C decomp.; ESI-MS: m/z: 426 [M]$^+$ (100%), 411 (21%), 397 (5%); ^{1}H and ^{13}C NMR chemical shifts are summarized in Tables 1 and 2 with exception for signals of the benzyl moiety. ^{1}H NMR: *CH*$_2$–Ar=4.76 ppm, CH_2–*Ar*=7.25–7.41 ppm; ^{13}C NMR: *CH*$_2$–Ar=56.97 ppm, CH_2–*Ar*=126.17, 126.76, 129.05 ppm.

4.5. General procedure for nucleophilic addition of nitrogen heterocycles to a quaternary protoberberine skeleton

A pear-shaped flame-dried flask (25 mL) with freshly distilled THF was charged with NaH (1.1 equiv) and nitrogen heterocycle (1 equiv) under argon atmosphere. The reaction mixture was sonicated for 15 min and after degassing, previously dried alkaloid (1 equiv) was added. The reaction mixture was then vigorously magnetically stirred at room temperature for several hours. When the suspension settled down, the organic phase was taken carefully through a syringe and in some cases filtered through HPLC filter and concentrated under vacuum. Products were usually obtained by crystallization in freezer.

*4.5.1. 8-(Pyrrol-1-yl)-7,8-dihydroberberine (**5a**).* Compound **5a** was prepared according to procedure described recently.[5]

*4.5.2. 8-(Indol-1-yl)-7,8-dihydroberberine (**5b**).* NaH (0.0220 g, 0.55 mmol), indole (0.0586 g, 0.5 mmol), and berberine chloride

(0.1859 g, 0.5 mmol) were used. Reaction mixture was magnetically stirred for 5 h.

Yield: 26% of brown solid; mp: ~200 °C decomp.; EIMS (30 eV): *m*/*z*: 336 [**1**]$^+$ (38%), 335 (42), 320 (61), 118 [indol+H]$^+$ (100); ^{1}H and ^{13}C NMR chemical shifts are summarized in Tables 1 and 2; IR (KBr, cm^{-1}) 3448, 2939, 2839, 1596, 1508, 1458, 1290, 1047, 746, 723, 433, 395, 389; HRMS (NALDI) *m*/*z* calculated for $C_{28}H_{23}N_2O_4$ (M−H$^•$) 451.1652, found 451.1650.

*4.5.3. 8-(3-Methylindol-1-yl)-7,8-dihydroberberine (**5c**).* NaH (0.0220 g, 0.55 mmol), 3-methylindole (0.0656 g, 0.5 mmol), and berberine chloride (0.1859 g, 0.5 mmol) were used. Reaction mixture was magnetically stirred for 5 h.

Yield: 43% brown solid, mp: ~200 °C decomp.; EIMS (30 eV): *m*/*z*: 337 (47%), 335 (48), 320 (54), 130 [3-methylindol+H]$^+$ (100); ^{1}H and ^{13}C NMR chemical shifts are summarized in Tables 1 and 2; IR (KBr, cm^{-1}) 3716, 2939, 1506, 1350, 1240, 757, 626, 513; HRMS (NALDI) *m*/*z* calculated for $C_{29}H_{25}N_2O_4$ (M−H$^•$) 465.1809, found 465.1802.

*4.5.4. 8-(Indazol-1-yl)-7,8-dihydroberberine (**5d**).* NaH (0.0220 g, 0.55 mmol), 1*H*-indazole (0.0591 g, 0.5 mmol), and berberine chloride (0.1859 g, 0.5 mmol) were used. Reaction mixture was magnetically stirred for 3 h.

Yield: 29% of brown solid, mp: ~175 °C decomp.; EIMS (30 eV): *m*/*z*: 335 (53), 334 (53), 320 (49), 118 [indazol+H]$^+$ (100); ^{1}H and ^{13}C NMR chemical shifts are summarized in Tables 1 and 2; IR (KBr, cm^{-1}) 3552, 3197, 3058, 2960, 2918, 1506, 1284, 615, 433, 399; HRMS (NALDI) *m*/*z* calculated for $C_{27}H_{22}N_3O_4$ (M−H$^•$) 452.1605, found 452.1601.

*4.5.5. 8-(Carbazol-1-yl)-7,8-dihydroberberine (**5e**).* NaH (0.0118 g, 0.259 mmol), carbazole (0.0449 g, 0.269 mmol), and berberine chloride (0.1859 g, 0.5 mmol) were used. Reaction mixture was magnetically stirred for 6 h.

Yield: 29% of yellow crystals; mp: 284 °C decomp.; EIMS (30 eV): *m*/*z*: 486 (17%), 471 (11), 336 [**1**]$^+$ (52), 320 (100), 319 (89); ^{1}H and ^{13}C NMR chemical shifts are summarized in Tables 1 and 2; IR (KBr, cm^{-1}) 3695, 3573, 2900, 1521, 381, 376, 372; HRMS (NALDI) *m*/*z* calculated for $C_{32}H_{25}N_2O_4$ (M−H$^•$) 501.1809, found 501.1807.

Crystal data[16] for **5e**: CCDC ref. No. 749835. Crystallized from THF, $C_{32}H_{26}N_2O_4$, M_{rel}=502.56, T=120 K, triclinic, space group $P\bar{1}$, a=6.9873(3) Å, b=10.4394(4) Å, c=16.5719(8) Å, α=98.067(4), β=92.521(4), γ=100.738(4), V=1172.83 Å^3, R=0.035.

*4.5.6. 8-(Carbazol-1-yl)-7,8-dihydropalmatine (**6e**).* NaH (0.006 g, 0.151 mmol), carbazole (0.0229 g, 0.137 mmol), and palmatine chloride (0.0532 g, 0.137 mmol) were used. Reaction mixture was magnetically stirred for 5 h.

Yield: 17%, pale yellow solid, mp: 146–155 °C decomp.; EIMS (30 eV): *m*/*z*: 352 [**3**]$^+$ (59%), 320 (40), 319 (49), 167 [carbazole+H]$^+$ (100); ^{1}H and ^{13}C NMR chemical shifts are summarized in Tables 1 and 2.

*4.5.7. 8-(Carbazol-1-yl)-7,8-dihydrocoptisine (**7e**).* Yield: 38%; mp: ~185 °C decomp.; EIMS (30 eV): *m*/*z*: 321 [**3**+H]$^+$ (54%), 167 [carbazol]$^+$ (100); ^{1}H and ^{13}C NMR chemical shifts are summarized in Tables 1 and 2; IR (KBr, cm^{-1}) 3311, 2900, 2852, 1506, 1488, 1282, 1029, 738, 696, 630, 474; HRMS (NALDI) *m*/*z* calculated for $C_{31}H_{21}N_2O_4$ (M−H$^•$) 485.1496, found 485.1485.

*4.5.8. 8-(Pyrrol-1-yl)-13-benzyl-7,8-dihydroberberine (**8a**).* NaH (0.0088 g, 0.22 mmol), pyrrole (13.8 μL, 0.2 mmol), and 13-benzylberberine bromide (0.1013 g, 0.2 mmol) were used. Reaction mixture was magnetically stirred for 4 h.

Yield: 47%, pale yellow solid, mp: 232.5 °C; EIMS (30 eV): *m*/*z*: 427 [M-pyrrol]$^+$ (54%), 336 [**1**]$^+$ (42), 320 (59), 68 [pyrrol+H]$^+$ (100); ^{1}H and ^{13}C NMR chemical shifts are summarized in Tables 1 and 2 with exception for signals of the benzyl moiety. ^{1}H NMR: CH_2–Ar=4.22 ppm, CH_2–*Ar*=7.21–7.38 ppm; ^{13}C NMR: CH_2–Ar=35.80 ppm, CH_2–*Ar*=126.62, 128.78, 129.34, 142.29 ppm; IR (KBr, cm^{-1}) 3413, 2929, 1483, 1274, 1238, 1060, 1047, 756, 727, 632, 445; HRMS (NALDI) *m*/*z* calculated for $C_{31}H_{27}N_2O_4$ (M−H$^•$) 491.1965, found 491.1963.

4.6. Theoretical calculations

All the calculations were performed with the GAUSSIAN 03[17] package of programs. Geometries were optimized at the B3LYP[18] level of theory with the 3-21G(d) or 6-31G(d) basis set when necessary. In the case of a flat potential energy surface near the minimum, where the optimization procedure using the approximate Hessian matrix was terminated prior to full convergence, force constants were calculated analytically. Harmonic vibrational frequencies were computed for all stationary points to provide thermal correction to Gibbs free energy at 298 K and 1 atm. Finally, single point energies for the B3LYP geometries were computed at the B3LYP level of theory with the 6-311+G(2d,p) basis set. Transition structures (TS) on the potential energy surface were located by using the facility of GAUSSIAN for the synchronous transit-guided quasi-Newton method.[19]

The NMR shielding tensors were calculated on the gas phase geometries with the B3LYP/6-31G(d,p) level of theory using the GIAO[20] procedure. Self-consistent reaction field (SCRF) calculations were performed to simulate the solvent effects in this case. The polarized continuum model (PCM) of Tomasi and co-workers[21] with CH_2Cl_2 (ϵ=8.93) as a solvent was used. The final chemical shifts were obtained with respect to tetramethylsilane.

Nucleus-independent chemical shift (NICS) calculations were performed by applying GIAO method at HF/6-31G* level of theory in GAUSSIAN 03. Three-dimensional matrixes of dummy atoms in Cartesian coordinates (with spacing of 0.1 Å) were created for the *iso*-NICS surface analysis.[10b] Differential *iso*-NICS surface was created as a difference between the *iso*-NICS surface for carbazole and that for indole. Calculated differential *iso*-NICS surface was then projected into the coordination system of compound **5e**. Differential *iso*-NICS surfaces were visualized by using Molekel software.[22]

Acknowledgements

The authors would like to thank Professor Jiří Dostál for his gift of plant material from *Chelidonium majus* (mixture of QPAs), Dr. Lubomír Prokeš for his help with measuring the EI mass spectra and Dr. Karel Šmejkal for measuring the ESI mass spectra. The financial support of the Ministry of Education of the Czech Republic (MSM0021622413 and LC06030 to L.M., M.P., Z.K., and R.M.) is gratefully acknowledged. Gratitude is also expressed to the Department of Chemistry of the University of Fribourg for use of their computer facilities. The computational resources were partially provided by MetaCentrum, Czech Republic (grant MSM6383917201).

Supplementary data

Supplementary data associated with this article can be found in the online version at doi:10.1016/j.tet.2010.09.030. These data include MOL files and InChIKeys of the most important compounds described in this article.

References and notes

1. (a) Grycová, L.; Dostál, J.; Marek, R. *Phytochemistry* **2007**, *68*, 150; (b) Bentley, K. W. *The Isoquinoline Alkaloids*; Harwood Academic: Amsterdam, 1998, pp 219–259;

(c) *The Protoberberines and Retroprotoberberines The Isoquinoline Alkaloids*; Shamma, M., Ed.; Academic: New York, NY, London, 1972, pp 268–314; (d) Bhakuni, D. S.; Jain, S. Protoberberine alkaloids. In *The Alkaloids*; Academic: New York, NY, 1986, pp 95–181.
2. (a) Iwasa, K.; Kamigauchi, M.; Ueki, M.; Taniguchi, M. *Eur. J. Med. Chem.* **1996**, *31*, 469; (b) Park, D. K.; Lee, H. J.; Kim, H. S.; Kang, H. T.; Moon, S. J.; Kim, S. U. *Bioorg. Med. Chem. Lett.* **2006**, *16*, 3913; (c) Hayashi, K.; Minoda, K.; Nagaoka, Y.; Hayashi, T.; Uesato, S. *Bioorg. Med. Chem. Lett.* **2007**, *17*, 1562; (d) Iwasa, K.; Nishiyama, Y.; Ichimaru, M.; Moriyasu, M.; Kim, H. S.; Wataya, Y.; Yamori, T.; Takashi, T.; Lee, D. U. *Eur. J. Med. Chem.* **1999**, *34*, 1077; (e) McCall, C. L. D.; Alexander, J.; Barber, J.; Jaouhari, G. R.; Satoskar, A.; Waigh, R. D. *Bioorg. Med. Chem. Lett.* **1994**, *4*, 1663; (f) Iwasa, K.; Kim, H. S.; Wataya, Y.; Lee, D. U. *Eur. J. Med. Chem.* **1998**, *33*, 65.
3. (a) Pilch, S. D.; Yu, C.; Makhey, D.; LaVoie, E. J.; Srinivasan, A. R.; Olson, K. W.; Sauers, R. R.; Breslauer, K. J.; Geacintov, N. E.; Liu, F. L. *Biochemistry* **1997**, *36*, 12542; (b) Mazzini, S.; Belluci, C. M.; Mondelli, R. *Bioorg. Med. Chem.* **2003**, *11*, 505; (c) Bhadra, K.; Maiti, M.; Kumar, G. S. *Biochim. Biophys. Acta* **2008**, *1780*, 1054; (d) Chen, W.; Qin, Y.; Cai, Z.; Chan, C. *Bioorg. Med. Chem.* **2005**, *13*, 1859; (e) Maiti, M.; Kumar, G. S. *Med. Res. Rev.* **2007**, *27*, 649.
4. (a) Iwasa, K.; Lee, D. U.; Kang, S. I.; Wiegrebe, W. *J. Nat. Prod.* **1998**, *61*, 1150; (b) Vennerstrom, J. L.; Klayman, L. D. *J. Med. Chem.* **1988**, *31*, 1184; (c) Marek, R.; Sečkářová, P.; Hulová, D.; Marek, J.; Dostál, J.; Sklenář, V. *J. Nat. Prod.* **2003**, *66*, 481; (d) Dostál, J.; Man, S.; Sečkářová, P.; Hulová, D.; Nečas, M.; Potáček, M.; Toušek, J.; Dommisse, R.; van Dongen, W.; Marek, R. *J. Mol. Struct.* **2004**, *687*, 135.
5. Grycová, L.; Hulová, D.; Maier, L.; Standara, S.; Nečas, M.; Lemière, F.; Kareš, R.; Dostál, J.; Marek, R. *Magn. Reson. Chem.* **2008**, *46*, 1127.
6. Bain, D. A. *Annu. Rep. NMR Spectrosc.* **2008**, *63*, 23.
7. (a) Anand, A.; Roy, D. A.; Chakrabarty, R.; Saxena, K. A.; Roy, R. *Tetrahedron* **2007**, *63*, 5236; (b) Aguirre, G.; Somanatan, R.; Hellberg, H. L.; Dwyer, J. T.; North, R. *Magn. Reson. Chem.* **2003**, *41*, 131; (c) Santos, D.; Suardiaz, R.; Montero, A. L.; Pérez, C. *J. Mol. Struct., THEOCHEM* **2008**, *852*, 78.
8. Friebolin, H. *Basic One and Two Dimensional NMR Spectroscopy*, 3rd ed.; Wiley VCH: Weinheim, 1998, pp 301–329.
9. Wiitala, K. W.; Cramer, J. C.; Hoye, T. R. *Magn. Reson. Chem.* **2007**, *45*, 819.
10. (a) Schleyer, P. v. R.; Maerker, C.; Dransfeld, A.; Jiao, H. J.; Hommes, N. J. R. V. *J. Am. Chem. Soc.* **1996**, *118*, 6317; (b) Klod, S.; Kleinpeter, E. *J. Chem. Soc., Perkin Trans. 2* **2001**, 1893; (c) Morgan, D.; Manoharan, M.; Heine, T.; Schleyer, P. v. R. *Org. Lett.* **2003**, *5*, 23; (d) Kleinpeter, E.; Koch, A. *Tetrahedron* **2009**, *65*, 5350; (e) Kleinpeter, E.; Koch, A. *J. Phys. Chem. A* **2010**, *114*, 5928; (f) Shainyan, B. A.; Fettke, A.; Kleinpeter, E. *J. Phys. Chem. A* **2008**, *112*, 10895.
11. Jeener, J.; Meier, B. H.; Bachmann, P.; Ernst, R. R. *J. Chem. Phys.* **1979**, *71*, 4546.
12. Müller, L. *J. Am. Chem. Soc.* **1979**, *101*, 4481.
13. Willker, W.; Leibfritz, D.; Kerssebaum, R.; Bermel, W. *Magn. Reson. Chem.* **1993**, *31*, 287.
14. Marek, R.; Králík, L.; Sklenář, V. *Tetrahedron Lett.* **1997**, *38*, 665.
15. SHELXTL. *Version 5.10*; Bruker AXS: Madison, WI, USA, 1997.
16. Crystallographic data for the structure reported in this paper have been deposited with the Cambridge Crystallographic Data Centre. Copies of the data can be obtained, free of charge, on application to CCDC, 12 Union Road, Cambridge CB2 1EZ, UK (fax: +44 1223 336033 or e-mail: deposit@ccdc.cam.ac.uk).
17. Frisch, M. J. T.; Trucks, G. W.; Schlegel, H. B.; Scuseria, G. E.; Robb, M. A.; Cheeseman, J. R.; Montgomery, J. A., Jr.; Vreven, T.; Kudin, K. N.; Burant, J. C.; Millam, J. M.; Iyengar, S. S.; Tomasi, J.; Barone, V.; Mennucci, B.; Cossi, M.; Scalmani, G.; Rega, N.; Petersson, G. A.; Nakatsuji, H.; Hada, M.; Ehara, M.; Toyota, K.; Fukuda, R.; Hasegawa, J.; Ishida, M.; Nakajima, T.; Honda, Y.; Kitao, O.; Nakai, H.; Klene, M.; Li, X.; Knox, J. E.; Hratchian, H. P.; Cross, J. B.; Bakken, V.; Adamo, C.; Jaramillo, J.; Gomperts, R.; Stratmann, R. E.; Yazyev, O.; Austin, A. J.; Cammi, R.; Pomelli, C.; Ochterski, J. W.; Ayala, P. Y.; Morokuma, K.; Voth, G. A.; Salvador, P.; Dannenberg, J. J.; Zakrzewski, V. G.; Dapprich, S.; Daniels, A. D.; Strain, M. C.; Farkas, O.; Malick, D. K.; Rabuck, A. D.; Raghavachari, K.; Foresman, J. B.; Ortiz, J. V.; Cui, Q.; Baboul, A. G.; Clifford, S.; Cioslowski, J.; Stefanov, B. B.; Liu, G.; Liashenko, A.; Piskorz, P.; Komaromi, I.; Martin, R. L.; Fox, D. J.; Keith, T.; Al-Laham, M. A.; Peng, C. Y.; Nanayakkara, A.; Challacombe, M.; Gill, P. M. W.; Johnson, B.; Chen, W.; Wong, M. W.; Gonzalez, C.; Pople, J. A. *Gaussian 03*; Gaussian: Wallingford CT, 2003.
18. Becke, A. D. *J. Chem. Phys.* **1993**, *98*, 5648.
19. Peng, C.; Ayala, P. Y.; Schlegel, H. B.; Frisch, M. J. *J. Comput. Chem.* **1996**, *17*, 49.
20. (a) Ditchfield, R. *Mol. Phys.* **1974**, *27*, 789; (c) Wolinski, K.; Hinton, J. F.; Pulay, P. *J. Am. Chem. Soc.* **1990**, *112*, 8251.
21. (a) Miertus, S.; Scrocco, E.; Tomasi, J. *Chem. Phys.* **1981**, *55*, 117; (b) Miertus, S.; Tomasi, J. *Chem. Phys.* **1982**, *65*, 239; (c) Tomasi, J.; Mennucci, B.; Cammi, R. *Chem. Rev.* **2005**, *105*, 2999.
22. Flukiger, P.; Portmann, S. *Molekel 4.3*; Swiss Center for Scientific Computing: Switzerland, 2002.